Microsegregation Behavior during Solidification and Homogenization of AerMet100 Steel

H.E. LIPPARD, C.E. CAMPBELL, T. BJÖRKLIND, U. BORGGREN, P. KELLGREN, V.P. DRAVID, and G.B. OLSON

Cast AerMet100 exhibits mechanical properties comparable to the wrought properties of competing ultrahigh-strength steels; however, the segregation behavior had not been quantified under casting conditions. A microsegregation profile of the as-cast ingot was simulated and homogenization treatments were predicted using Thermo-Calc and DICTRA software. Experimental composition analysis confirmed the simulated microsegregation profile, and the homogenization process occurred at a slightly faster rate than predicted. The convergence of theory and experiment demonstrates the feasibility of designing cast alloy compositions assisted by computer simulation to minimize segregation without casting a large experimental matrix of test ingots.

I. INTRODUCTION/BACKGROUND

AERMET100* is a commercial high-alloy steel produced in wrought forms by Carpenter Technology, Inc. for applications requiring a combination of high strength, high fracture toughness, and resistance to stress-corrosion cracking.[1] The nominal composition is (wt pct) 13.4 pct Co, 11.1 pct Ni, 3.1 pct Cr, 1.2 pct Mo, 0.23 pct C, and the balance Fe. Standard mechanical property specifications for the wrought alloy are 2065 MPa UTS, 1860 MPa YS, and 132 MPa$\sqrt{\text{m}}$ K_{IC}. The alloy is produced by vacuum-induction melting (VIM) and vacuum-arc remelting (VAR) to ensure the very low impurity levels necessary to achieve the property specifications. The possibility of industrial applications using cast AerMet100 was sparked by the remarkably high mechanical properties obtained from VIM quality-control test ingots prior to VAR processing. Strength and toughness properties of the homogenized and tempered VIM castings were found to be equal or superior to the wrought properties of the high-strength steels Marage 250, 300M, H11, and 4340.[2]

This investigation explored the applicability of using thermodynamic/kinetic modeling software to predict microsegregation of the as-cast material and the optimal homogenization treatment to eliminate microsegregation. Most of the previous work[3–13] in the field of compositional analysis and, particularly, in the modeling of microsegregation has been limited to ternary and a few quaternary systems. Recent studies have included six or more elements by thermodynamic modeling of superalloys.[14] The software used for this investigation was able to model fully the effects of the six major constituents of this commercial alloy on microsegregation. Macrosegregation was not included in the computer simulation models.

To predict the microsegregation in a multicomponent alloy requires both multicomponent thermodynamic phase descriptions and diffusion coefficients. The SGTE[15] database, as implemented in the Thermo-Calc**[16,17] program (version K), uses the CALPHAD method to extrapolate thermodynamic descriptions for use in an n-component system based on the assessment of binary and available ternary and quaternary experimental data. The thermodynamics of the liquid phase are described by a regular solution model and the solid phases by the sublattice model.[18] The phase equilibria are calculated by a free-energy minimization determined by a Newton–Raphson technique. The CALPHAD method has been extended by Jönsson[19] to the assessment of concentration-dependent diffusion coefficients in multicomponent alloys and is implemented in the mobility database.[20] Thermodynamic and kinetic data are combined in the DICTRA[21,22] software (version 18) to simulate diffusion-controlled transformations. The DICTRA system assumes that local equilibrium exists at the moving phase interface and that the flux-balance Eq. [1] is obeyed.

$$v^{\alpha}\, c_k^{\alpha} - v^{\beta}\, c_k^{\beta} = J_k^{\alpha} - J_k^{\beta} \qquad k = 1,2...,n \qquad [1]$$

where v^{α} and v^{β} are the interface velocities with respect to the local frames of reference in the α and β phases. The terms c^{α} and c^{β} are the concentrations at the phase interface, and J_k^{α} and J_k^{β} are the corresponding diffusional fluxes. For an n-component system at a specified temperature and pressure, the number of conditions needed to determine a unique tie-line is $n - 2$. Under equilibrium conditions, this tieline is chosen using mass balance constraints. When phase transformation/diffusional equilibria are considered, the unique tie-line must satisfy the flux-balance equations. Solutions to the diffusion Eq. [2] and local equilibrium at the phase interface are used to determine the tieline that solves the flux-balance equations employing a finite-difference method.

$$\frac{\partial c_k}{\partial t} = -\text{div}\, J_k \quad J_k = \sum_{j=1}^{n-1} D_{kj}^{n}\, \nabla c_j = \sum_{j=1}^{n} L'_{kj}\, \nabla \mu_j \qquad [2]$$

where D_{kj}^{n} is the diffusion-coefficient matrix for a given phase when species n is chosen as the solvent, and L'_{kj} is a phenomenological parameter defined in the volume-fixed frame of reference by Anderson and Agren[21] and Kirkaldy and Young.[23] In the lattice-fixed frame of reference, the

H.E. LIPPARD, C.E. CAMPBELL, Graduate Students, V.P. DRAVID, and G.B. OLSON, Professors, are with the Department of Materials Science and Engineering, Northwestern University, Evanston, IL 60208. T. BJÖRKLIND, U. BORGGREN, and P. KELLGREN, Students, are with the Division of Computational Thermodynamics, Royal Institute of Technology, Stockholm, Sweden S-100 44.

Manuscript submitted January 22, 1997.

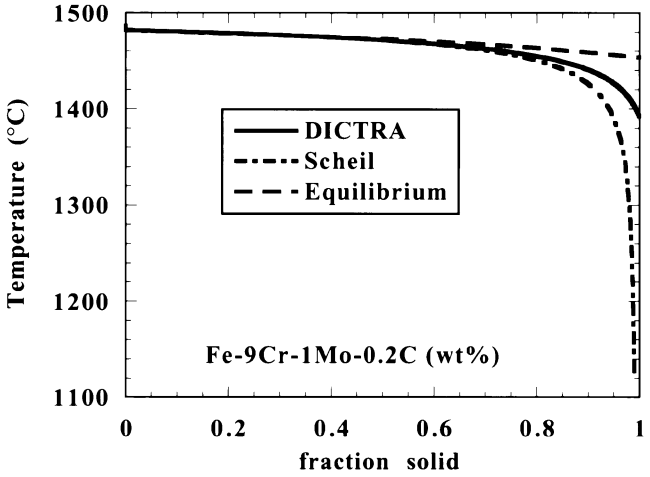

Fig. 1—Comparison of simulation models for the fraction solid as a function of temperature for the alloy Fe-9Cr-1Mo-0.2C (wt pct).

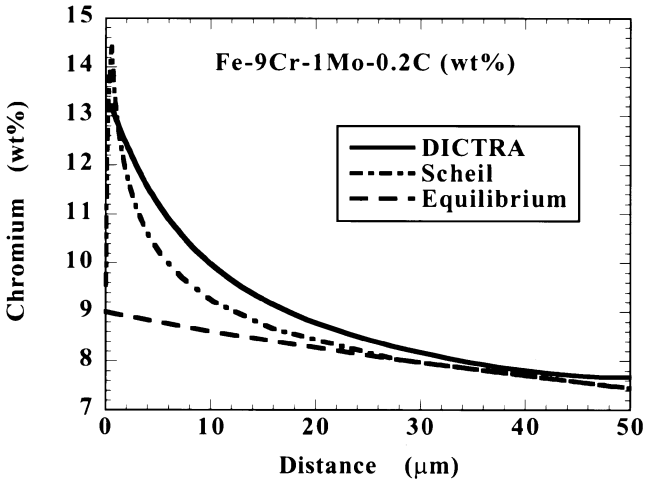

Fig. 2—Comparison of simulation models for chromium composition as a function of space in a 100-μm secondary dendrite arm for the alloy Fe-9Cr-1Mo-0.2C (wt pct).

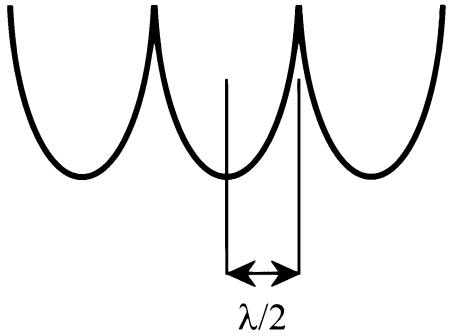

Fig. 3—Secondary dendrite arm spacing.

off-diagonal terms of the L matrix are not considered, as their contribution is expected to be small.[23] However, the off-diagonal terms of the diffusion matrix, in the volume-fixed frame of reference, are considered.

There are three general approaches to modeling the microsegregation in a multicomponent alloy. The simplest method assumes that equilibrium is always preserved; thus, infinitely slow cooling is implied and homogeneous liquid and solid compositions are maintained. The upper bound on the degree of microsegregation is predicted using the Scheil analysis,[24] which allows no diffusion in the solid phase and presumes perfect mixing in the liquid phase. A more realistic model assumes that equilibrium is only maintained at the liquid/solid interface and allows diffusion in both the solid and liquid phases; such a model is implemented in the DICTRA software. Figure 1, temperature *vs* the fraction solidified, demonstrates the differences between the three models by considering the solidification of the model alloy Fe-9Cr-1Mo-0.2C (wt pct). The Scheil analysis predicts a much greater solidification range than the equilibrium or DICTRA simulations. Chromium composition profiles calculated by the three models (Figure 2) show the large difference in the degree of microsegregation predicted by the Scheil and DICTRA models relative to the equilibrium simulation. The Scheil and DICTRA simulations diverge in the final solidification region, where the Scheil model predicts the formation of a carbide while the DICTRA model displays a continuous increase in chromium content to the final solidification point.

Using DICTRA to simulate the solidification process of AerMet100, several assumptions were made. The alloy composition was assumed to be Fe-13.3Co-11.1Ni-3.0Cr-0.9Mo-0.23C (wt pct), based on average compositional analysis acquired from energy dispersive spectroscopy (EDS) data collected from a large field-of-view ($\approx$3 $\times$ 3 mm), long live-time scan corresponding to the region where morphological information was obtained. The simulation composition reduced chromium and molybdenum levels slightly to 3.0 and 0.9 wt pct, respectively, to compensate for the extensive macrosegregation to the central core.

The computational domain of the simulation was defined as the half-width of the secondary dendrite arm spacing and was approximated at 50 μm (Figure 3). The computational grid consisted of 100 points spaced on a geometric series weighted to increase resolution at the cell boundaries where the rate of composition change was highest. Referring to the work of Flemings *et al.*,[7] who measured a primary dendrite arm spacing of 160 μm and secondary dendrite arm spacing 70 μm for a Fe-1.5Cr-1.0C (wt pct) alloy cooled at a rate of 0.57 °C/s, a cooling rate of 0.5 °C/s was chosen. A planar geometry at the liquid/solid interface was assumed. The starting temperature for the solidification process was 25 °C higher than the equilibrium melting temperature predicted by Thermo-Calc (1464 °C). The initial liquid composition was assumed to be homogeneous and equal to nominal alloy composition. Two solidification reactions were considered: liquid -> fcc and liquid -> fcc + MC carbide. The solidification was simulated allowing diffusion in both the liquid and solid phases.

The composition profiles from the solidification process defined the initial composition profiles for the homogenization simulations. The simulations considered only diffusion in the fcc phase.

II. EXPERIMENTAL PROCEDURE

The sample for this study was a 1.5 $\times$ 1.5 $\times$ 10 cm ingot from a sand casting of AerMet100 prepared at Carpenter Technology, Inc. Standard metallographic polishing procedures were used to prepare the sample prior to etch-

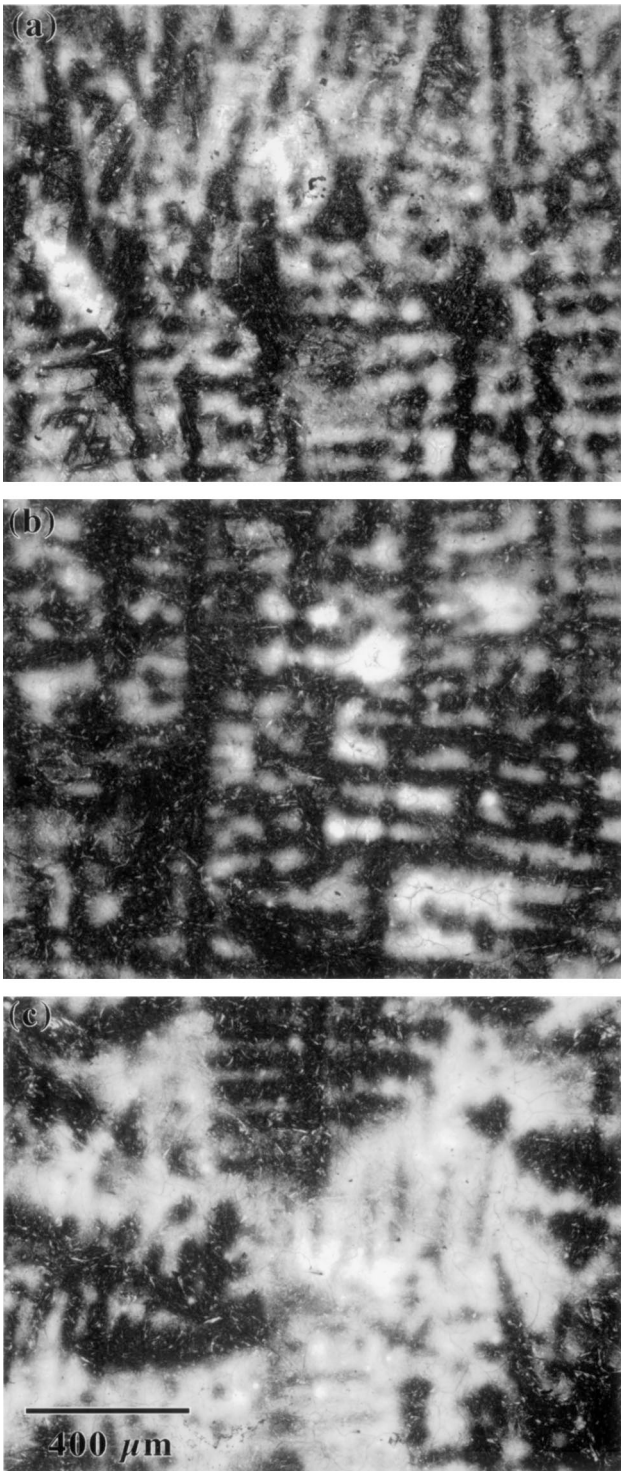

Fig. 4—Optical micrographs of the as-cast AerMet100 dendritic structure at the (*a*) ingot edge, (*b*) ingot midpoint, and (*c*) central core region.

ing. A macroetch solution of 50 pct HCl-50 pct H_2O at 80 °C revealed the dendritic structure for study in both optical and electron microscopes. Homogenization treatments were conducted in a tube furnace at 1177 °C (±5 °C) for 14 and 36 hours with samples vacuum encapsulated in quartz tubing. The samples were oil quenched after homogenization. Analytical composition data was acquired using an Hitachi S-4500 cold field emission scanning electron microscope (SEM) with a Noran EDS detector and Voyager software. Composition data was collected at a 30 kV accelerating voltage to ensure sufficient overvoltage of all alloy elements, and the emission current was 20 μA, resulting in a high count rate on the order of 2000 counts per second. Spectra were acquired for a live time of 60 seconds or more, and proper flashing of the field emission filament prior to a linescan prevented problems associated with emission current decay.

Composition analysis was conducted using automated line profile software to acquire, store, and quantitatively fit an EDS spectrum for each data point on the line. Peak deconvolution of the overlapped iron, cobalt, and nickel K lines was accomplished by multiple linear least-squares fitting with single-element standards. The fitting procedure was checked against known standards and compared with other peak deconvolution methods for accuracy. The alternate curve-fitting techniques were inadequate with respect to consistent treatment of the convoluted K peaks.

The simulations were performed on a Sun Sparc5 workstation serving multiple users. The DICTRA solidification calculations were the most computationally intensive and ranged in computer time from 3 hours for a four-component solidification to 12 hours for the full six-component simulation. The Scheil and homogenization simulations required less than 30 minutes.

III. RESULTS/DISCUSSION

Figure 4 shows the fernlike pattern of the as-cast dendritic structure. The primary dendrite arm spacing ranged from 150 μm in the chill zone to 400 μm in the central region, and the secondary dendrite spacing varied from 70 to 110 μm over the same regions. The dendrite arm spacing remained constant through most of the ingot body at 300 μm for primary arms and 100 μm for secondary arms. Higher order dendrite arms were not visible in the microstructure. The final solidification region, the central core covering ≈0.02 area fraction of the specimen, displayed no evidence of dendritic structure. Prior austenite grain boundaries were observed in the solute-rich central core and dark interdendritic regions, but were obscured in the more heavily etched solute-poor dendrite arms.

Homogenization at 1177 °C for 14 and 36 hours resulted in large blocky light and dark regions with no apparent relationship to the prior dendritic structure. The morphology is too large in scale to correspond to either the prior austenite grains or the lath structure of the martensite matrix. The macrosegregated central core region retained its size and shape. Required etching times compared to the as-cast material increased by an order of magnitude, indicating a reduction in microsegregation.

The macroetch used was not particularly suited for revealing microstructure; however, a few microscale observations were made from secondary electron (SE) images in the SEM. The solute-rich core and interdendritic regions etched very smoothly, and prior austenite grain boundaries had a ridge of material denoting their location in the as-cast material. The surface roughness of the heavily etched, solute-poor dendrite arms precluded identification of microscale phenomena. The microstructure of the homogenized samples was also difficult to interpret because of surface roughness. There were no clearly identifiable grain

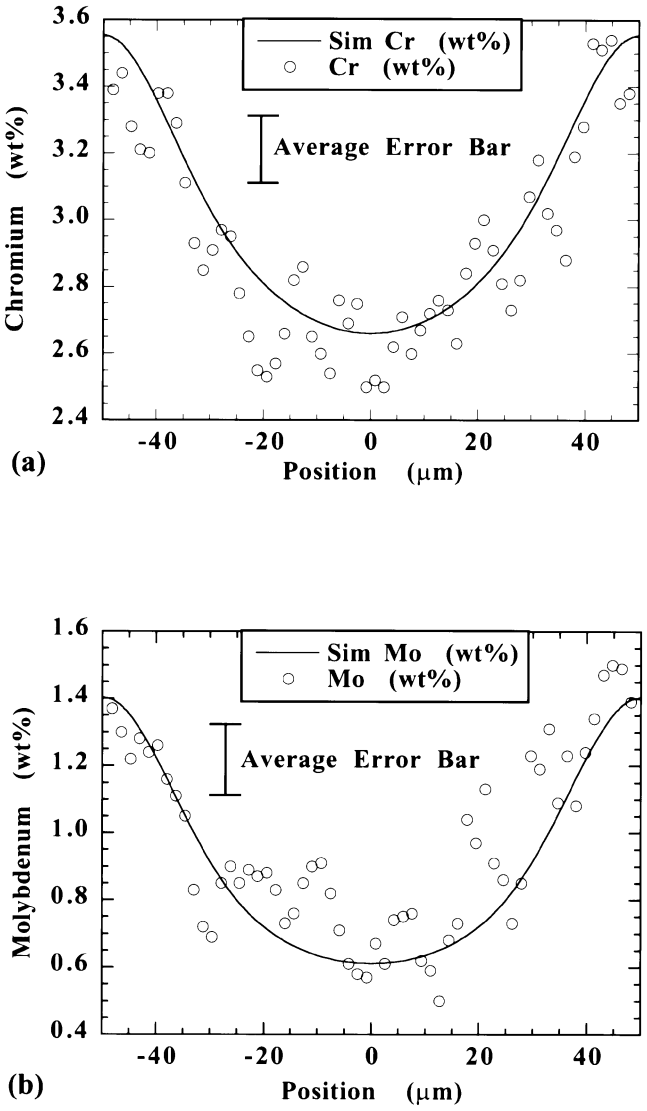

Fig. 5—Experimental and DICTRA simulated line profile compositions for as-cast AerMet100 across a 100-μm secondary dendrite arm for (*a*) chromium and (*b*) molybdenum.

boundaries or lath structures in the SE images, except in the central core region. Several microetchants were applied to freshly polished surfaces of both as-cast and homogenized specimens, but none revealed new microstructural information. The microetchants reproduced the macroetch effects after long application times. The lack of second phases is not unexpected because the homogenization temperature is higher than the carbide-forming temperatures, and the relatively rapid solidification conditions prevent carbides from forming during the cooling stage.

The exceptional agreement between the experimental composition profiles across secondary dendrite arms and the solidification simulation for chromium and molybdenum is shown in Figure 5. The experimental data scatter relative to the simulation does exceed the average error bounds for several points. Examination of the chromium and molybdenum residuals does not reveal a clear correlation, which would be indicative of large carbides forming during the solidification process. Several microetchants were employed to reveal carbides in the as-cast material, but all were unsuccessful at exposing a second phase. Surface features intercepting the X-rays generated in the direct beam interaction volume is a possible explanation of the scatter in the heavily etched regions where the anomalous points occurred. Nickel segregated with chromium and molybdenum while cobalt exhibited no discernible segregation pattern. The simulations also showed that carbon microsegregation had the same waveform as chromium and varied from 0.25 to 0.22 wt pct; however, experimental quantitative carbon analysis was not feasible due to surface contamination.

Table I. Elemental Segregation Indices, δ, of Simulations and Experimental Data for AerMet100 in the As-Cast and Homogenized Conditions

Condition	Element	δ_{exp}	δ_{DICTRA}	δ_{Scheil}
As-cast	Mo	2.08	2.26	7.58
	Cr	1.33	1.34	2.89
	Ni	1.10	1.10	1.41
	Co	1.00	1.04	1.20
	C	?	1.12	17.1
14 h	Mo	1.15	1.65	—
	Cr	1.03	1.20	—
36 h	Mo	1.00	1.15	—
	Cr	1.01	1.07	—

Experimental and simulated segregation indices ($\delta = C_{max}/C_{min}$) are summarized in Table I. In comparison to the 50-deg freezing zone calculated by DICTRA, the Scheil simulation predicted a larger freezing zone of 362 deg. The large freezing zone resulted from the assumptions that the liquid is perfectly mixed and there is no diffusion in the solid phase; therefore, solidification did not occur until an eutectic temperature was reached. The Scheil simulation's delay in solidification allowed for carbide formation, which led to the high segregation ratio for *C*. The DICTRA simulation predicted no carbide formation.

The homogenization treatments obscured the dendritic structure and complicated the visual selection of analysis points. A random distribution of data points was employed to locate the remnants of dendritic structure and to select a suitable region for linescans. The results for both heat treatment cycles are summarized in Figure 6 with the as-cast data. The rate of homogenization is slightly faster than predicted by the simulations, indicating a need for further multicomponent database development and refining of homogenization models. The error is most likely due to multicomponent interaction effects on the mobility of chromium and molybdenum, which have not been experimentally determined for Fe-Co-X systems. The molybdenum mobility is estimated to be 2.6 times lower than that for iron in the fcc phase.[21] The faster rate of homogenization resulted in prediction errors of 10 pct for chromium and 15 pct for molybdenum concentration after 14 hours at 1173 °C, suggesting that the chromium and molybdenum mobilities are somewhat greater than originally assessed for an Fe-Co-Ni alloy.

Macrosegregation to the ingot central core was measured by large-area scans encompassing large fractions of the central region and by point acquisitions. The scans are represented in Figure 7 by the core average data, and the core

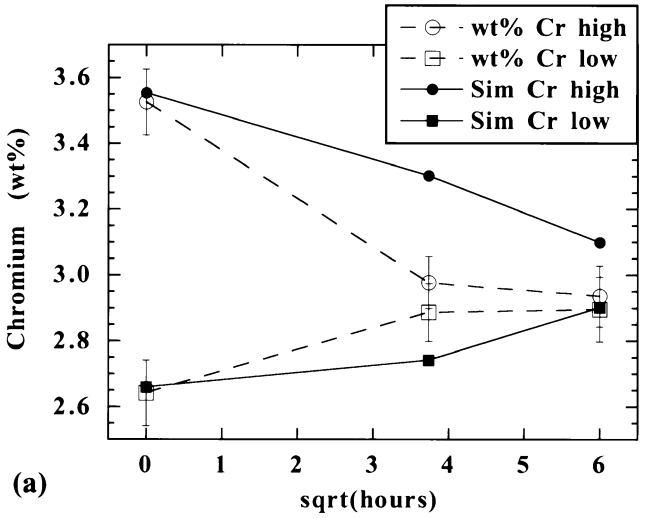

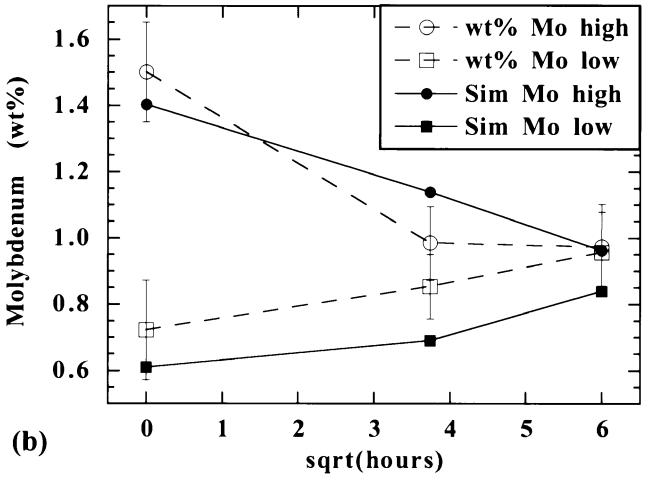

Fig. 6—Experimental and DICTRA simulated maximum/minimum dendrite compositions for AerMet100 as a function of homogenization time at 1173 °C for (*a*) chromium and (*b*) molybdenum.

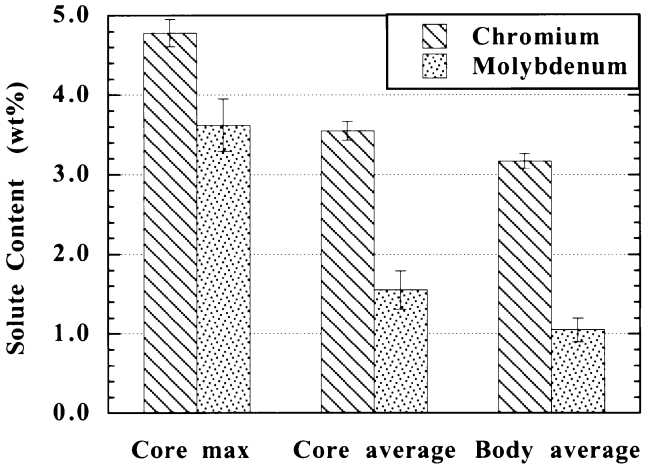

Fig. 7—Macrosegregation of chromium and molybdenum to the central core of the cast ingot.

maximum values are point acquisitions. The final macrosegregation level increases with larger ingot size and slower cooling rate. The macrosegregation results are of limited applicability since they are not valid for all ingot sizes and casting conditions. However, minimization of microsegregation would also reduce the macrosegregation level, allowing the casting of relatively large part sizes at moderate cooling rates. The homogenization treatments employed did not reduce the core macrosegregated region, nor would any practical heat treatment.

IV. CONCLUSIONS

The simulation of the cast AerMet100 microsegregation composition profile by the DICTRA software was very successful. The thermodynamic and kinetic parameters and their interactions were accurately modeled such that the simulation data quantitatively matched with the experimental results. The procedure for this investigation can be extended to the design of new multicomponent cast alloys where sufficient thermodynamic data has been collected to minimize the microsegregation without analyzing a large matrix of experimental test ingots.

The simulation of the homogenization treatment predicted slower kinetics than were found experimentally. The difference is attributed to uncertainty in the mobility of molybdenum in iron. Full homogenization (<5 pct deviation) of the microsegregation was achieved in less than 36 hours at 1173 °C, but the macrosegregation level in the casting core was not reduced by the homogenization treatments.

While the Scheil model correctly predicts the major segregates, it overestimates the degree of microsegregation. The degree of error in the Scheil analysis could be reduced by including back diffusion in the model, as seen in the work of Knatter *et al.*[14] The DICTRA simulation accurately simulates the solidification process and the degree of microsegregation; however, it did require a substantial increase in computing time. The DICTRA system's capability to accurately simulate the solidification process and other diffusional processes is dependent on the accuracy of the thermodynamic and kinetic data.

The ability to predict the degree of microsegregation in a multicomponent alloy is an important design tool. Through simulations of the solidification process that systematically vary alloying additions, the positive and negative cross-compositional effects on the degree of microsegregation can be determined, allowing predictive control of this aspect of castability.

ACKNOWLEDGMENTS

This research was initiated as an international student collaboration between materials design classes at Northwestern University and the Royal Institute of Technology, Stockholm. DICTRA calculations at Stockholm were supervised by Bo Jansson and Bo Sundman with assistance from Mikael Lindholm, Lars Höglund, and Mikael Schalin. Research on AERMET100 steel at Northwestern University is supported by ARO under Grant No. DAAH04-93-G-0471/P01 and NSF Graduate Student Fellowship support given to HEL and CEC.

REFERENCES

1. P.M. Novotny: *Gilbert R. Speich Symp. Proc.*, TMS, Warrendale, PA, 1992, pp. 215-36.
2. P.M. Novotny and M. Maguire: *Foundry Manag. Technol.*, 1993, vol. 121, pp. 33-36.
3. T.W. Clyne and W. Kurz: *Metall. Trans. A*, 1981, vol. 12A, pp. 965-71.
4. T.Z. Kattamis and M.C. Flemings: *Trans. TMS-AIME*, 1965, vol. 233, pp. 992-99.
5. H.D. Brody and M.C. Flemings: *Trans. TMS-AIME*, 1966, vol. 236, pp. 615-24.
6. T.F. Brower, H.D. Brody, and M.C. Flemings: *Trans. TMS-AIME*, 1966, vol. 236, pp. 624-34.
7. M.C. Flemings, D.R. Poirier, R.V. Barone, and H.D. Brody: *J. Iron Steel Inst.*, 1970, vol. 208, pp. 371-81.
8. J. Philibert, E. Weinryb, and M. Ancey: *Metallurgia*, 1965, vol. 72, pp. 203-11.
9. R.D. Doherty and D.A. Melford: *J. Iron Steel Inst.*, 1966, vol. 204, pp. 1131-43.
10. H. Thresh, M. Bergeron, F. Weinberg, and R.K. Buhr: *Trans. TMS-AIME*, 1968, vol. 242, pp. 853-58.
11. S.V. Subramanian, C.W. Haworth, and D.H. Kirkwood: *J. Iron Steel Inst.*, 1968, vol. 206, pp. 1027-32.
12. B.A. Rickinson and D.H. Kirkwood: *Proc. Conf. on Solidification and Casting of Metals*, Metals Society, London, 1979, pp. 44-52.
13. D.H. Kirkwood: *Mater. Sci. Eng.*, 1984, vol. 65, pp. 101-09.
14. U.R. Kattner, W.J. Boettinger, and S.R. Coriell: *Z. Metallkd.*, 1996, vol. 87, pp. 522-28.
15. SGTE, Scientific Group Thermodata Europe.
16. B. Sundman, B. Jansson, and J.O. Andersson: *CALPHAD*, 1985, vol. 9, pp. 153-90.
17. THERMO-CALC, version K, Royal Institute of Technology, Stockholm, 1995.
18. B. Sundman and J. Ågren: *J. Phys. Chem. Solids*, 1981, vol. 42, pp. 297-301.
19. B. Jönsson: *Z. Metallkd.*, 1995, vol. 86, pp. 686-92.
20. *Mobility Database*, Royal Institute of Technology, Stockholm, 1995.
21. J.O. Andersson and J. Ågren: *J. Appl. Phys.*, 1992, vol. 72, pp. 1350-55.
22. *DICTRA*, version 18, Royal Institute of Technology, Stockholm, 1995.
23. J.S. Kirkaldy and D.J. Young: *Diffusion in the Condensed State*, The Institute of Metals, London, 1987, pp. 127-49.
24. E. Scheil: *Z. Metallkd.*, 1942, vol. 34, pp. 70-72.